LETTERS

Control of cortical GABA circuitry development by Nrg1 and ErbB4 signalling

Pietro Fazzari[1], Ana V. Paternain[1], Manuel Valiente[1], Ramón Pla[1], Rafael Luján[2], Kent Lloyd[3], Juan Lerma[1], Oscar Marín[1] & Beatriz Rico[1]

Schizophrenia is a complex disorder that interferes with the function of several brain systems required for cognition and normal social behaviour. Although the most notable clinical aspects of the disease only become apparent during late adolescence or early adulthood, many lines of evidence suggest that schizophrenia is a neurodevelopmental disorder with a strong genetic component[1,2]. Several independent studies have identified neuregulin 1 (*NRG1*) and its receptor *ERBB4* as important risk genes for schizophrenia[3,4], although their precise role in the disease process remains unknown. Here we show that Nrg1 and ErbB4 signalling controls the development of inhibitory circuitries in the mammalian cerebral cortex by cell-autonomously regulating the connectivity of specific GABA (γ-aminobutyric acid)-containing interneurons. In contrast to the prevalent view, which supports a role for these genes in the formation and function of excitatory synapses between pyramidal cells, we found that ErbB4 expression in the mouse neocortex and hippocampus is largely confined to certain classes of interneurons. In particular, ErbB4 is expressed by many parvalbumin-expressing chandelier and basket cells, where it localizes to axon terminals and postsynaptic densities receiving glutamatergic input. Gain- and loss-of-function experiments, both *in vitro* and *in vivo*, demonstrate that ErbB4 cell-autonomously promotes the formation of axo-axonic inhibitory synapses over pyramidal cells, and that this function is probably mediated by Nrg1. In addition, ErbB4 expression in GABA-containing interneurons regulates the formation of excitatory synapses onto the dendrites of these cells. By contrast, ErbB4 is dispensable for excitatory transmission between pyramidal neurons. Altogether, our results indicate that Nrg1 and ErbB4 signalling is required for the wiring of GABA-mediated circuits in the postnatal cortex, providing a new perspective to the involvement of these genes in the aetiology of schizophrenia.

Nrg1 has been linked to abnormal cortical functioning in schizophrenia[5,6], but the contribution of this signalling system to the development and function of specific circuits in the cerebral cortex has not been firmly established. The predominant view favours a role for Nrg1 and ErbB4 signalling at excitatory circuitries in the cortex[4,7–10]. However, ErbB4 expression has also been observed in hippocampal interneurons *in vitro*[11,12], and a subset of GABAergic terminals in the cerebral cortex express ErbB4 (ref. 13). Because no study has been able to reconcile these apparently conflicting findings, the precise place of action for Nrg1 and ErbB4 signalling in the postnatal cortex remains controversial.

Erbb4 messenger RNA (which encodes ErbB4 protein) is expressed by scattered cells throughout the neocortex and hippocampus in postnatal mice, in a pattern that resembles the distribution of interneurons (Supplementary Fig. 1). Thus, we analysed the pattern of ErbB4 expression in *Dlx5/6-Cre-IRES-GFP* (*Dlx5/6-Cre-i-GFP*) transgenic mice, in which virtually all forebrain GABAergic interneurons express green fluorescent protein (GFP). Analysis of ErbB4 expression with antibodies whose specificity was tested in *Erbb4* mutant mice (Supplementary Fig. 2) showed that most ErbB4-expressing cells in the cerebral cortex are interneurons (Fig. 1a, b and Supplementary Fig. 3). This suggested that few, if any, pyramidal neurons express ErbB4 in the mouse postnatal cortex. To confirm this, we prepared protein lysates from the cortex of interneuron-specific (IN) and pyramidal neuron-specific (PN) conditional *Erbb4* mutant mice, obtained by breeding *Dlx5/6-Cre* and *NEX-Cre* mouse strains, respectively, with mice homozygous for *loxP*-flanked (F) *Erbb4* alleles. We found that ErbB4 was barely detectable in cortical lysates obtained from *IN-Erbb4* mutants, whereas only minor differences were observed between *PN-Erbb4* mutants and controls (Fig. 1c). These results strongly support the view that ErbB4 expression in the cortex is largely restricted to GABAergic interneurons[14].

We next wondered what specific classes of cortical GABAergic interneurons express ErbB4 (Fig. 1e). We found that ErbB4 is expressed by many parvalbumin-expressing cortical interneurons, whereas only a small fraction of calretinin- and somatostatin-expressing interneurons contains this receptor (Fig. 1d, f and Supplementary Fig. 4). Consistently, ErbB4 localized to interneurons with the morphological features of chandelier and basket cells (19 out of 22 $ErbB4^+$ chandelier cells, and 203 out of 221 $ErbB4^+$ basket cells, two brains; Fig. 1g, h and Supplementary Fig. 5)—the two main classes of fast-spiking parvalbumin-expressing interneurons[15,16].

To determine the subcellular localization of ErbB4 in cortical interneurons, we performed pre-embedding immunogold electron microscopy in the hippocampus of postnatal day (P)30 wild-type mice. We found that ErbB4-bound gold particles were frequently associated with symmetric synapses (likely to use GABA as neurotransmitter) that contacted the cell body and axon initial segment (AIS) of hippocampal pyramidal cells (Fig. 1i and Supplementary Fig. 6a). Gold particles were more frequent in axon terminals contacting the AIS (11 positive axon terminals out of 32 counted, 10 different AISs) than those targeting the cell body (14 positive axon terminals out of 58 counted, 23 pyramidal cell somas). We did not observe gold particles within terminals associated with dendritic spines or shafts of pyramidal cells (0 positive axon terminals out of 523), corroborating that ErbB4 is not present at contacts established between pyramidal neurons (Supplementary Fig. 6b). To gain synaptic resolution, we next performed post-embedding immunogold electron microscopy. These experiments confirmed the absence of ErbB4 from excitatory synapses contacting other pyramidal neurons (0 positive axon terminals out of 722; Supplementary Fig. 6c). In contrast, we found that ErbB4-bound gold particles were present at

[1]Instituto de Neurociencias, Consejo Superior de Investigaciones Científicas & Universidad Miguel Hernández, 03550 Sant Joan d'Alacant, Spain. [2]Departamento Ciencias Médicas, Facultad de Medicina, Universidad de Castilla-La Mancha, 02006 Albacete, Spain. [3]Department of Internal Medicine, California National Primate Research Center, University of California, Davis, California 95616, USA.

©2010 Macmillan Publishers Limited. All rights reserved

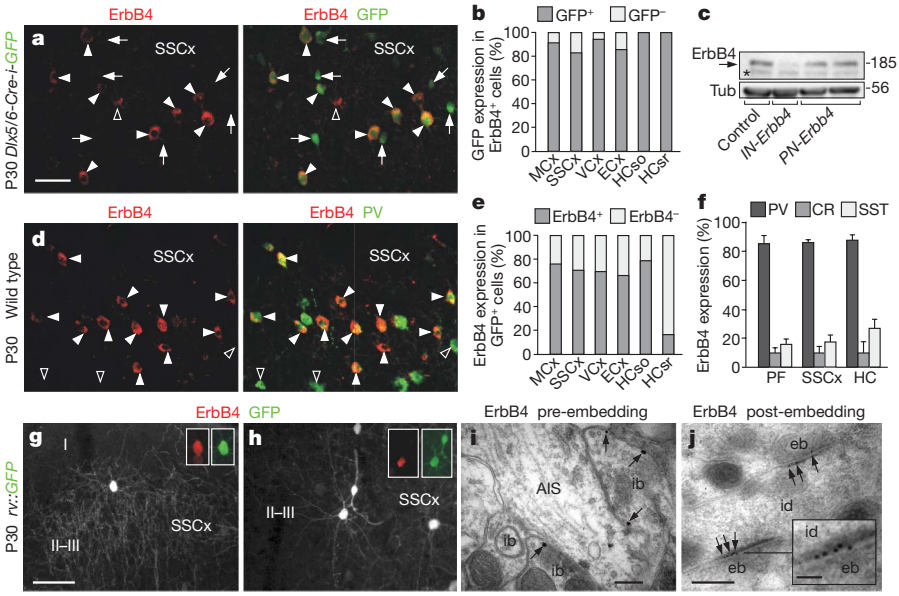

Figure 1 | ErbB4 is expressed by many interneurons in the postnatal neocortex and hippocampus, but not in pyramidal cells at P30. **a**, ErbB4 (filled and open arrowheads) and GFP (arrows and filled arrowheads) immunohistochemistry in the somatosensory cortex (SSCx) of a P30 *Dlx5/6-Cre* mouse. **b**, Percentage of interneurons among all ErbB4-expressing cortical cells. ECx, entorhinal cortex; HCso, hippocampus stratum oriens; HCsr, hippocampus stratum radiatum; MCx, motor cortex; VCx, visual cortex. **c**, Immunoblots of ErbB4 protein in the brains of control, *IN-Erbb4* and *PN-Erbb4* mutants (fold to control: *IN-Erbb4*, 8.6 ± 1.7%, $n = 3$; *PN-Erbb4*, 85.9 ± 1.3%, $n = 2$). Asterisk points to a non-specific band. Tub, tubulin loading control. **d**, Double immunohistochemistry for ErbB4 (filled arrowheads) and parvalbumin (PV; filled and open arrowheads) in the somatosensory cortex of a wild-type mouse. **e**, Percentage of ErbB4-expressing cells among all cortical interneurons. **f**, Percentage of ErbB4-expressing cells among different classes of cortical interneurons. Parvalbumin: prefrontal cortex (PF), 85 ± 5% (mean ± s.e.m.); SSCx, 86 ± 2%; hippocampus (HC), 88 ± 4%. Calretinin (CR): PF, 10 ± 4%; SSCx, 10 ± 5%; HC, 10 ± 7%. Somatostatin (SST): PF, 16 ± 4%; SSCx, 18 ± 5%; HC, 27 ± 6%; $n = 3$. **g**, **h**, Expression of ErbB4 in a chandelier (**g**) and basket (**h**) cell. I, layer I; II–III; layers II–III. **i**, **j**, Immunogold labelling (arrows) localizes ErbB4 to inhibitory boutons (ib) contacting the AIS of pyramidal neurons, and postsynaptic to excitatory boutons (eb) contacting the dendrites of interneurons (id) in hippocampus. Histograms show mean and s.e.m. Scale bars, 50 μm (**a**, **d**), 150 μm (**g**, **h**), 0.3 μm (**i**), 0.2 μm (**j**) and 0.05 μm (inset in **j**).

postsynaptic densities (PSDs) on dendritic shafts of interneurons (22 positive axon terminals out of 43, 10 dendritic shafts; Fig. 1j and Supplementary Fig. 6c). In sum, ErbB4 is expressed in GABAergic terminals contacting the soma and AISs of pyramidal neurons, as well as in PSDs of GABAergic dendrites receiving excitatory input.

As both type I/II (immunoglobulin-like domain (Ig-Nrg1); diffusible) and type III (cysteine-rich domain (CRD-Nrg1); membrane-bound) forms of Nrg1 are expressed in the postnatal cortex (Supplementary Fig. 1 and data not shown), we proposed that ErbB4-mediated Nrg1 signalling could influence the postnatal development of specific classes of GABAergic interneurons. To begin testing this hypothesis, we cultured hippocampal neurons from *GAD65-GFP* mice with medium supplemented with the purified Nrg1-β1. We found that interneurons cultured with Nrg1-β1 extend longer axons and have more branches compared to control medium (Fig. 2a–c).

To investigate whether Nrg1 promotes the formation of GABAergic synapses, we analysed hippocampal cultures transfected with plasmids encoding for either GFP or *CRD-Nrg1-IRES-GFP* (*CRD-Nrg1-i-GFP*). Because many parvalbumin-expressing basket cells contain ErbB4, and these interneurons preferentially form perisomatic synapses[17], we quantified the axonal density of GAD65-expressing boutons over the soma of transfected pyramidal cells. Compared to controls, pyramidal neurons overexpressing *CRD-Nrg1* showed significantly increased perisomatic innervation (Fig. 2d–h), suggesting that Nrg1 is sufficient *in vitro* to promote the formation of GABAergic boutons onto pyramidal neurons.

We next studied whether Nrg1 and ErbB4 signalling influences the formation of cortical GABAergic synapses *in vivo*. We first performed gain-of-function experiments by electroporating plasmids encoding for either GFP or *CRD-Nrg1-i-GFP* in cortical progenitor cells by *in utero* electroporation at embryonic day (E)14.5 (Fig. 2i). Analysis of these experiments at P30 showed that the expression of CRD-Nrg1 does not impair the radial migration of transfected pyramidal neurons (Supplementary Fig. 7). We found, however, that the density of GAD65 boutons formed onto the soma of pyramidal neurons expressing CRD-Nrg1 almost doubled that found in neurons expressing only GFP (Fig. 2j, m, l). In addition, we found that overexpression of *CRD-Nrg1* also increases the number of GAD65 boutons targeting the AIS (Fig. 2k, l, n), which is preferentially innervated by chandelier cells[18]. Thus, Nrg1 promotes the development of perisomatic and AIS GABAergic innervation of pyramidal neurons *in vivo*.

We performed loss-of-function experiments *in vivo* to determine whether ErbB4 mediates the function of Nrg1 in the formation of GABAergic synapses. To scrutinize the cell-autonomous function of ErbB4, we performed ultrasound imaging to focally inject a cocktail of two retroviruses—one encoding for the Cre recombinase and GFP (*GFP-i-Cre*) and another for monomeric red fluorescent protein (mRFP)—in E13.5 *Erbb4*$^{F/F}$ embryos (Fig. 3a). Viruses were placed into the medial ganglionic eminence (MGE), the main origin of parvalbumin-expressing interneurons[19]. Simultaneous infection with both retroviruses allowed us to study both wild-type and *Erbb4* mutant interneurons in the same cortical regions of the same mice. Short-term control experiments showed normal tangential migration of interneurons expressing *GFP-i-Cre*, probably due to the perdurance of ErbB4 protein during the early phases of migration (Supplementary Fig. 8 and Methods). Nevertheless, analysis of the postnatal cortex at P30 showed that Cre was expressed by all GFP-expressing neurons ($n = 20$ cells; Supplementary Fig. 9), and that Cre had efficiently eliminated *Erbb4* from all GFP-positive basket or chandelier cells ($n = 20$ cells; Supplementary Fig. 9).

We focused our analysis on neocortical chandelier cells because the morphology of their axons is highly stereotyped, which facilitates the consistent comparison of mutant and control cells. We did not find any systematic difference in the gross morphology of wild-type and *Erbb4* mutant chandelier cells (Fig. 3b, f and Supplementary Fig. 10). Similarly, the average length of candlesticks (characteristic terminal portions of the chandelier cell axon) as well as their relative density per cell did not differ between control and mutant cells (Fig. 3c–e, g,

©2010 Macmillan Publishers Limited. All rights reserved

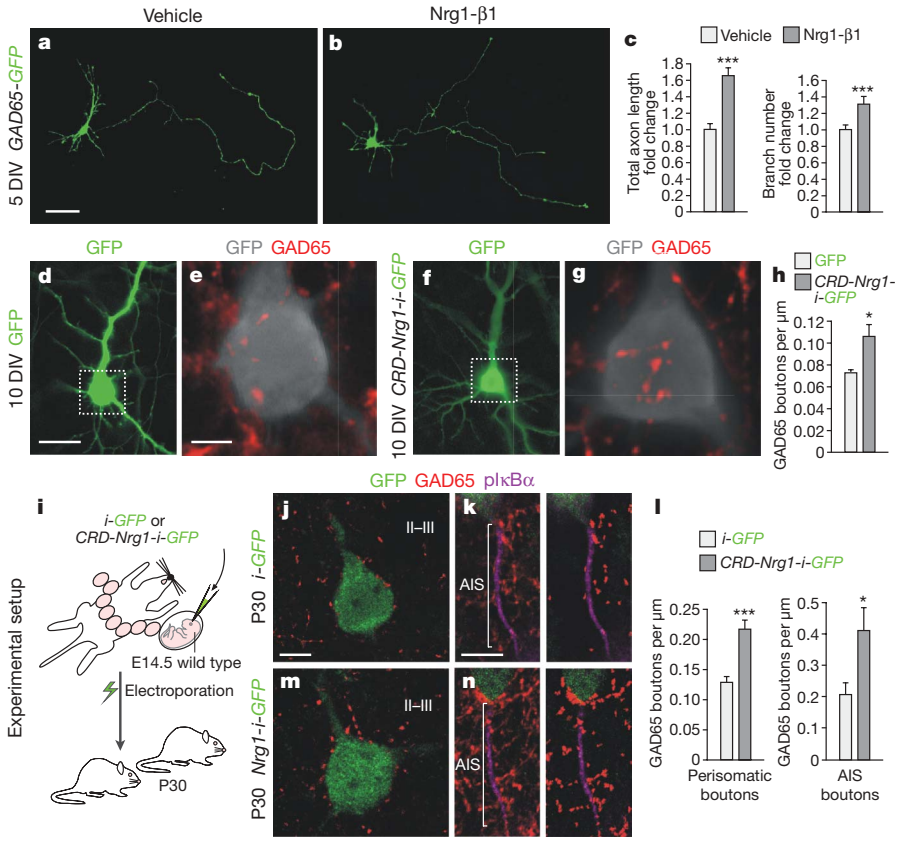

Figure 2 | Nrg1 promotes GABAergic differentiation and synaptogenesis. **a**, **b**, Hippocampal interneurons from primary cultures treated with control medium or Nrg1-β1 at 5 days *in vitro* (DIV). **c**, Fold change in total axonal length and number of branches in hippocampal interneurons treated with Nrg1-β1 compared to controls. Control, $n = 78$; Nrg1-β1, $n = 92$, three cultures; $***P < 0.001$, Mann–Whitney test. **d**–**g**, Distribution of GAD65-positive boutons contacting the soma of transfected hippocampal pyramidal neurons. **h**, Number of GAD65 boutons per axonal length; $n = 50$ neurons, five cultures; $*P < 0.05$, *t*-test. **i**, Experimental model. **j**, **k**, **m**, **n**, Single confocal images showing GAD65 boutons apposed to the soma and AIS of transfected pyramidal neurons. ImageJ software was used to process AIS images for counting (**k** (right) and **n** (right)). **l**, Density of GAD65 boutons. Perisomatic: GFP, $n = 24$; *CRD-Nrg1*, $n = 35$ neurons, four brains. AIS: GFP, $n = 26$; *CRD-Nrg1*, $n = 30$ neurons, four brains. $*P < 0.05$, $***P < 0.001$, *t*-test. Scale bars, 50 μm (**a**, **b**), 25 μm (**d**, **f**), and 5 μm (**e**, **g**, **j**, **k**, **m**, **n**). Histograms show mean and s.e.m.

h). In contrast, analysis of the density of boutons made by chandelier cell axons showed a significant decrease in *Erbb4* mutant cells compared to controls (Fig. 3c–e, g, h). Because these boutons contain GAD65 (Supplementary Fig. 11), these results demonstrated that the loss of ErbB4 in cortical interneurons cell-autonomously impairs their ability to establish GABAergic synapses.

We reasoned that if Nrg1 and ErbB4 signalling contributes to the establishment of GABAergic synapses, then conditional mutants lacking ErbB4 from cortical interneurons (*IN-Erbb4*) should perhaps display functional abnormalities. To test this hypothesis, we first performed control experiments to verify that early development of GABAergic interneurons was not compromised in *IN-Erbb4* mutants. We found that tangential migration of interneurons was largely unaffected in *IN-Erbb4* mutants, probably due to perdurance of ErbB4 protein during the transition of interneurons from the subpallium to the pallium (Supplementary Fig. 12). Consistently, the total number of hippocampal GABAergic interneurons and the number and layer distribution of those that express parvalbumin were similar in control and *IN-Erbb4* mutant mice (Supplementary Fig. 13). We next measured synaptic activity with whole-cell recordings from hippocampal CA1 pyramidal neurons in acute slices obtained from P20 control and *IN-Erbb4* mutant mice (Fig. 3i). Analysis of miniature inhibitory currents (mIPSCs) showed a significant decrease in the frequency of synaptic events in *IN-Erbb4* mutants compared to controls (Fig. 3j–l). In contrast, no change in the amplitude of mIPSCs was detected between both experimental groups (Fig. 3j, m). The reduction in the frequency of mIPSCs could be caused by a decrease in the number of release sites, a decrease in the probability of GABA release, or both. To distinguish between these possibilities, we studied whether loss of ErbB4 signalling influences the release properties of GABAergic synaptic terminals. We analysed pair-pulse ratios in control and *IN-Erbb4* mutants and found no differences between both experimental groups (Supplementary Fig. 14). Altogether, these results indicate that Nrg1 and ErbB4 signalling controls the formation and/or maintenance of GABAergic synapses on pyramidal cells, and that presynaptic ErbB4 function seems to be required for this process.

To unequivocally rule out a role for ErbB4 in excitatory synapses between pyramidal neurons, we performed two further sets of experiments. First, we deleted *Erbb4* from pyramidal cells by infecting the lateral ventricle of $Erbb4^{F/F}$ embryos with a cocktail of retroviruses expressing *GFP-i-Cre* or mRFP to label clones of *Erbb4* mutant or control pyramidal cells, respectively. Analysis of the density of dendritic spines in wild-type and *Erbb4* mutant pyramidal cells showed no significant differences (Supplementary Fig. 15). Second, we evaluated synaptic function by whole-cell recordings from hippocampal CA1 pyramidal neurons in acute slices obtained from control and *PN-Erbb4* mutant mice (Supplementary Fig. 16). Analysis of miniature excitatory currents (mEPSCs) showed no significant differences in the frequency or amplitude of these synaptic events in *PN-Erbb4* mutants compared to controls (Supplementary Fig. 16). Thus, even if expressed in some pyramidal cells, elimination of ErbB4 from these neurons does not seem to disrupt excitatory transmission in pyramidal–pyramidal synapses.

The finding of ErbB4 at PSDs in GABAergic interneuron dendrites indicated that this signalling system could have a role in the formation of excitatory inputs to these cells. To test this hypothesis, we performed whole-cell recordings from interneurons located in the stratum oriens and stratum pyramidale of hippocampus CA1 in acute slices obtained from P20 control and *IN-Erbb4* mutant mice (Fig. 4a). Analysis of miniature excitatory currents (mEPSCs) showed a significant decrease in the frequency of these events in *IN-Erbb4* mutants compared to controls (Fig. 4b–d). In contrast, no change in the amplitude of mEPSCs was detected between both experimental groups (Fig. 4b, e). In addition, analysis of the synaptic activity between pyramidal cells showed no differences in the frequency or amplitude of mEPSCs in *IN-Erbb4* mutants compared to controls (Supplementary Fig. 17), which demonstrated that excitatory connections are not generally disrupted in these mice.

These results indicated that postsynaptic ErbB4 expression is required for the formation of a normal complement of excitatory synapses on the dendrites of hippocampal interneurons. Analysis of the distribution of mEPSCs frequencies recorded from control

©2010 Macmillan Publishers Limited. All rights reserved

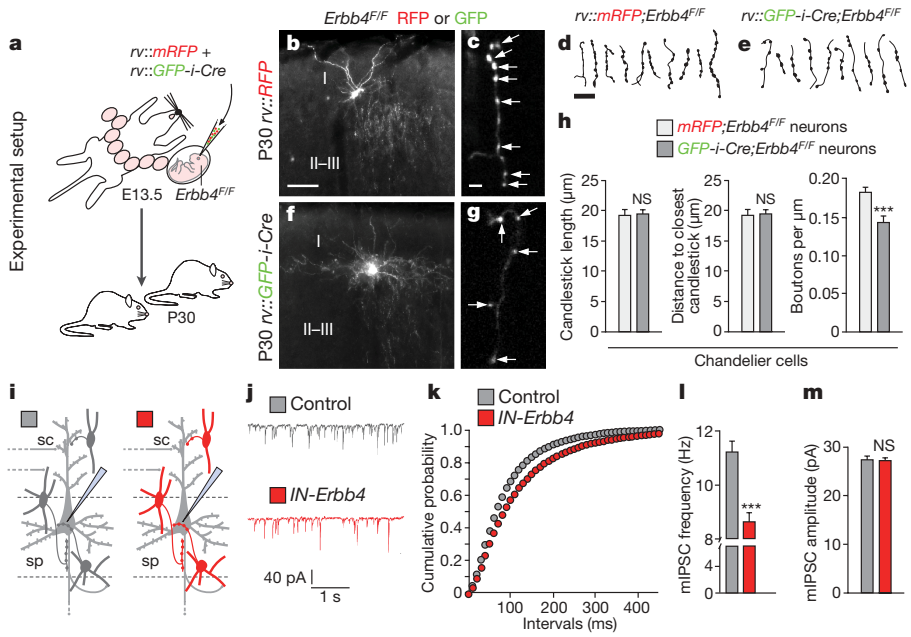

Figure 3 | Nrg1 and ErbB4 signalling is necessary for inhibitory synapse formation *in vivo*. **a**, Experimental model. **b**, **f**, Representative wild-type and *Erbb4* mutant chandelier cells in the somatosensory cortex. **c**, **g**, Representative candlesticks. Arrows point to axonal boutons. **d**, **e**, Drawings from representative candlesticks from ten wild-type (**d**) and *Erbb4* mutant (**e**) chandelier cells. **h**, Length of candlestick ($P = 0.90$), distance to the closest candlestick ($P = 0.81$), and density of boutons (0.1840 ± 0.0052 and 0.1440 ± 0.0079 boutons per µm for wild-type and *Erbb4* mutant cells, respectively). $^{***}P < 0.001$, *t*-test. NS, not significant. Control: $n = 11$ neurons, 374 candlesticks; *Erbb4* mutant: $n = 10$ neurons, 276 candlesticks, four brains. **i**, Experimental model. sc, Schaffer collaterals; sp, stratum pyramidale. **j**–**m**, Representative traces (**j**), cumulative plot (**k**) and measurements of mIPSC frequencies (**l**) and mIPSC amplitudes (**m**). Control: $n = 50$ neurons, three brains; *Erbb4* mutant: $n = 71$ neurons, four brains. $^{***}P < 0.001$ (**l**), $P = 0.70$ (**m**), *t*-test. Scale bars, 100 µm (**b**, **f**), 10 µm (**d**), and 2 µm (**c**, **g**). Histograms show mean and s.e.m.

interneurons showed great variability (Fig. 4f), with some neurons receiving many more inputs than others. Parvalbumin$^+$ cells are thought to receive the strongest excitatory drive among the different interneuron populations[20], and this particular population seemed to be missing in *IN-Erbb4* mice (Fig. 4f). To confirm this, we analysed the number of excitatory terminals, as identified by VGlut-1 immunohistochemistry, contacting hippocampal parvalbumin-expressing interneurons in control and *IN-Erbb4* mutants. We found a significant reduction in the density of VGlut-1-expressing terminals in *IN-Erbb4* mutants compared to controls (Fig. 4g–i). Altogether, these experiments demonstrated that ErbB4 also controls the formation and/or maintenance of excitatory synapses on specific populations of GABAergic interneurons, and that postsynaptic ErbB4 function is probably required in this process.

The mechanisms underlying the formation of inhibitory circuits in the cerebral cortex are poorly understood, and only a few molecules have so far been identified that participate in this process. Although the precise contribution of presynaptic and postsynaptic ErbB4 in this process remains to be determined, our experiments demonstrate that ErbB4 signalling controls the development of GABAergic circuits in the cerebral cortex at two different levels. First, ErbB4 signalling cell-autonomously contributes to the formation of perisomatic and axo-axonic synapses. Nrg1 is the probable mediator of this effect, although other neuregulins that bind ErbB4 and are expressed in the postnatal cortex, such as Nrg3, may also contribute. Second, ErbB4 is required for the formation and/or maintenance of excitatory synapses onto GABAergic interneurons. These results challenge the prevailing view of the function of Nrg1 and ErbB4 signalling in glutamatergic transmission between pyramidal cells[4,7–10], which is fundamentally based on the reported association between ErbB4 and PSD95 (refs 21, 22). Our finding that ErbB4 localizes to the postsynaptic density of glutamatergic synapses contacting the dendrites of inhibitory interneurons reconciles both sets of data, as it defines the precise site of action for Nrg1 and ErbB4 signalling in glutamatergic transmission.

Nrg1 and *Erbb4* are schizophrenia-susceptibility genes[4], but strong evidence for their aetiological role in the disorder is lacking. Considering that certain cognitive abnormalities in schizophrenia seem to reflect defects in specific cortical inhibitory circuits[23], the present findings contribute to understanding how deregulation of these genes may predispose individuals to disease. In particular, our results demonstrate that the loss of ErbB4 function in the mouse reduces the number of synapses made by chandelier cells, which is one of the most salient pathological features of individuals with schizophrenia[24]. In addition, postsynaptic ErbB4 expression is also required for parvalbumin-expressing interneurons to receive a normal complement of excitatory synapses. The function of these neurons

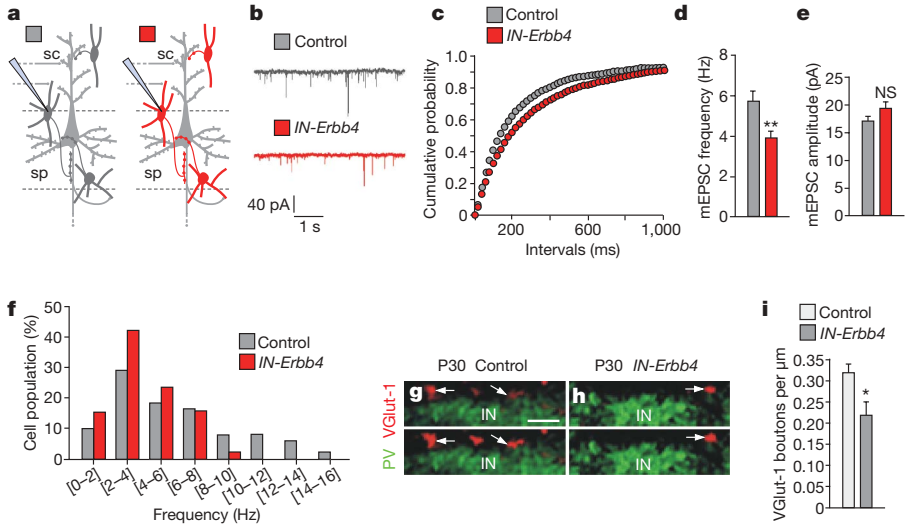

Figure 4 | Conditional deletion of *Erbb4* disrupts excitatory input to hippocampal interneurons. **a**, Experimental model. **b**–**e**, Representative traces (**b**), cumulative plot (**c**) and measurements of mEPSC frequencies (**d**) and mEPSC amplitudes (**e**). Control: $n = 48$ neurons, five brains; *Erbb4* mutant: $n = 38$ neurons, four brains. $^{**}P < 0.01$ (**d**), $P = 0.07$ (**e**), *t*-test. **f**, Analysis of the distribution of mEPSC frequencies recorded from hippocampal interneurons in control and *IN-Erbb4* mutants. $P < 0.01$, Welch test for the entire distribution. 0–5 Hz: $P < 0.05$; 5–16 Hz: $P < 0.01$, χ^2 test. **g**, **h**, Single confocal images showing VGlut-1 boutons apposed to parvalbumin-expressing hippocampal interneurons. ImageJ software was used to process images for counting (**g**, **h**, bottom). **i**, Density of VGlut-1 boutons. Control: $n = 17$, three brains; *IN-Erbb4* mutant: $n = 21$ neurons, three brains. $^{*}P < 0.05$, *t*-test. Scale bar, 1 µm (**g**, **h**). Histograms show mean and s.e.m.

©2010 Macmillan Publishers Limited. All rights reserved

is intimately linked to the generation of gamma-frequency synchronization[25–27]—an emergent property of cortical circuits that is linked to information processing and working memory in normal individuals[28] and the disruption of which contributes to the cognitive deficits of schizophrenia[29]. Moreover, although the contribution of the defects reported here to specific behavioural deficits remains to be experimentally tested, mice carrying various types of mutations for *Nrg1* and *Erbb4* display behavioural deficits that have been tentatively associated to schizophrenia[3,4]. On the basis of the observation that complete loss of Nrg1 and ErbB4 signalling disrupts interneuron development at earlier stages[30], it is tempting to speculate that different genetic alterations in this pathway may lead to diverse cortical interneuron deficits depending on their severity, and that this may contribute to increase phenotypic variability in schizophrenia.

METHODS SUMMARY

The 0618 rabbit anti-ErbB4 antibody was a gift from C. Lai. Null and floxed alleles for *Erbb4*, the Cre allele for the *Nex* locus, as well as *Dlx5/6-Cre-i-GFP*, $HER4^{heart}$ and *GAD65-GFP* transgenic mice have been described elsewhere (see details in Methods). *IN-Erbb4* and *PN-Erbb4* conditional mutants were obtained by crossing $Erbb4^{F/F}$ mice with *Dlx5/6-Cre*;$Erbb4^{F/+}$ and $Nex^{Cre/+}$;$Erbb4^{F/+}$ mice, respectively. For *in utero* infection, retroviruses expressing *GFP-i-Cre* or mRFP were injected directly into the MGE using ultrasound-guided imaging (VisualSonics). Control experiments were performed to verify that interneuron migration to the pallium was normal in both retroviral experiments and in *IN-Erbb4* mutants (see details in Methods), probably due to ErbB4 protein perdurance. Electron microscopic examination of ErbB4 immunoreactivity was performed using pre-and postembedding methods. Quantification of immunogold stainings was performed in single sections, and therefore our analysis probably underestimates the total number of labelled terminals. Hippocampal neurons were stimulated with recombinant NRG1-β1 (PeproTech EC) or transfected with Lipofectamine 2000. For electrophysiology, transverse hippocampal slices (300 μm) were prepared from P19–21 mice. Animals were kept under Spanish and EU regulation.

Full Methods and any associated references are available in the online version of the paper at www.nature.com/nature.

Received 7 August 2009; accepted 16 February 2010.
Published online 14 April 2010.

1. Lewis, D. A. & Levitt, P. Schizophrenia as a disorder of neurodevelopment. *Annu. Rev. Neurosci.* **25,** 409–432 (2002).
2. Owen, M. J., Williams, N. M. & O'Donovan, M. C. The molecular genetics of schizophrenia: new findings promise new insights. *Mol. Psychiatry* **9,** 14–27 (2004).
3. Stefansson, H. *et al.* Neuregulin 1 and susceptibility to schizophrenia. *Am. J. Hum. Genet.* **71,** 877–892 (2002).
4. Mei, L. & Xiong, W. C. Neuregulin 1 in neural development, synaptic plasticity and schizophrenia. *Nature Rev. Neurosci.* **9,** 437–452 (2008).
5. Addington, A. M. *et al.* Neuregulin 1 (8p12) and childhood-onset schizophrenia: susceptibility haplotypes for diagnosis and brain developmental trajectories. *Mol. Psychiatry* **12,** 195–205 (2007).
6. Hall, J. *et al.* A neuregulin 1 variant associated with abnormal cortical function and psychotic symptoms. *Nature Neurosci.* **9,** 1477–1478 (2006).
7. Barros, C. S. *et al.* Impaired maturation of dendritic spines without disorganization of cortical cell layers in mice lacking NRG1/ErbB signaling in the central nervous system. *Proc. Natl Acad. Sci. USA*. doi:10.1073/pnas.0900355106 (24 February 2009).
8. Bjarnadottir, M. *et al.* Neuregulin1 (NRG1) signaling through Fyn modulates NMDA receptor phosphorylation: differential synaptic function in $NRG1^{+/-}$ knock-outs compared with wild-type mice. *J. Neurosci.* **27,** 4519–4529 (2007).
9. Kwon, O. B., Longart, M., Vullhorst, D., Hoffman, D. A. & Buonanno, A. Neuregulin-1 reverses long-term potentiation at CA1 hippocampal synapses. *J. Neurosci.* **25,** 9378–9383 (2005).
10. Li, B., Woo, R. S., Mei, L. & Malinow, R. The neuregulin-1 receptor erbB4 controls glutamatergic synapse maturation and plasticity. *Neuron* **54,** 583–597 (2007).
11. Krivosheya, D. *et al.* ErbB4-neuregulin signaling modulates synapse development and dendritic arborization through distinct mechanisms. *J. Biol. Chem.* **283,** 32944–32956 (2008).
12. Longart, M., Chatani-Hinze, M., Gonzalez, C. M., Vullhorst, D. & Buonanno, A. Regulation of ErbB-4 endocytosis by neuregulin in GABAergic hippocampal interneurons. *Brain Res. Bull.* **73,** 210–219 (2007).
13. Woo, R. S. *et al.* Neuregulin-1 enhances depolarization-induced GABA release. *Neuron* **54,** 599–610 (2007).
14. Vullhorst, D. *et al.* Selective expression of ErbB4 in interneurons, but not pyramidal cells, of the rodent hippocampus. *J. Neurosci.* **29,** 12255–12264 (2009).
15. Klausberger, T. & Somogyi, P. Neuronal diversity and temporal dynamics: the unity of hippocampal circuit operations. *Science* **321,** 53–57 (2008).
16. Markram, H. *et al.* Interneurons of the neocortical inhibitory system. *Nature Rev. Neurosci.* **5,** 793–807 (2004).
17. Tamás, G., Buhl, E. H. & Somogyi, P. Fast IPSPs elicited via multiple synaptic release sites by different types of GABAergic neurone in the cat visual cortex. *J. Physiol. (Lond.)* **500,** 715–738 (1997).
18. Somogyi, P., Freund, T. F. & Cowey, A. The axo-axonic interneuron in the cerebral cortex of the rat, cat and monkey. *Neuroscience* **7,** 2577–2607 (1982).
19. Wonders, C. P. & Anderson, S. A. The origin and specification of cortical interneurons. *Nature Rev. Neurosci.* **7,** 687–696 (2006).
20. Gulyás, A. I., Megias, M., Emri, Z. & Freund, T. F. Total number and ratio of excitatory and inhibitory synapses converging onto single interneurons of different types in the CA1 area of the rat hippocampus. *J. Neurosci.* **19,** 10082–10097 (1999).
21. Garcia, R. A., Vasudevan, K. & Buonanno, A. The neuregulin receptor ErbB-4 interacts with PDZ-containing proteins at neuronal synapses. *Proc. Natl Acad. Sci. USA* **97,** 3596–3601 (2000).
22. Huang, Y. Z. *et al.* Regulation of neuregulin signaling by PSD-95 interacting with ErbB4 at CNS synapses. *Neuron* **26,** 443–455 (2000).
23. Lewis, D. A., Hashimoto, T. & Volk, D. W. Cortical inhibitory neurons and schizophrenia. *Nature Rev. Neurosci.* **6,** 312–324 (2005).
24. Woo, T. U., Whitehead, R. E., Melchitzky, D. S. & Lewis, D. A. A subclass of prefrontal gamma-aminobutyric acid axon terminals are selectively altered in schizophrenia. *Proc. Natl Acad. Sci. USA* **95,** 5341–5346 (1998).
25. Cardin, J. A. *et al.* Driving fast-spiking cells induces gamma rhythm and controls sensory responses. *Nature* **459,** 663–667 (2009).
26. Fuchs, E. C. *et al.* Recruitment of parvalbumin-positive interneurons determines hippocampal function and associated behavior. *Neuron* **53,** 591–604 (2007).
27. Sohal, V. S., Zhang, F., Yizhar, O. & Deisseroth, K. Parvalbumin neurons and gamma rhythms enhance cortical circuit performance. *Nature* **459,** 698–702 (2009).
28. Jensen, O., Kaiser, J. & Lachaux, J. P. Human gamma-frequency oscillations associated with attention and memory. *Trends Neurosci.* **30,** 317–324 (2007).
29. Spencer, K. M. *et al.* Abnormal neural synchrony in schizophrenia. *J. Neurosci.* **23,** 7407–7411 (2003).
30. Flames, N. *et al.* Short- and long-range attraction of cortical GABAergic interneurons by neuregulin-1. *Neuron* **44,** 251–261 (2004).

Supplementary Information is linked to the online version of the paper at www.nature.com/nature.

Acknowledgements We thank G. Fernández for technical assistance, T. Gil and A. Casillas for general laboratory support, C. Lai for antibodies and plasmids, F. H. Gage for retroviral vectors, and K. Campbell (*Dlx5/6-Cre-IRES-GFP*), M. Gassmann ($HER4^{heart}$ and $Erbb4^{-}$), S. Goebbels and K.-A. Nave (Nex^{Cre}), and G. Szabó (*GAD65-GFP*) for mouse strains. We are grateful to L. Menéndez de la Prida and P. Aivar for help with electrophysiological experiments, M. Maravall for critical reading of the manuscript, and members of the Borrell, Marín and Rico laboratories for stimulating discussions and ideas. This work was supported by grants from Spanish Ministry of Science and Innovation SAF2008-00770 (to O.M.), SAF2007-61904 (to B.R.), BFU2006-07138 (to J.L.), and CONSOLIDER CSD2007-00023 (to J.L., O.M. and B.R.), Consejería de Educación y Ciencia de la Junta de Comunidades de Castilla-La Mancha PAI08-0174-6967 (to R.L.), fundació la Caixa (to B.R.) and the EURYI (see http://www.esf.org/euryi) scheme award (to O.M). P.F. is the recipient of a Marie Curie Intra-European Fellowship.

Author Contributions P.F., O.M. and B.R. planned the experiments, and P.F. analysed the results. A.V.P. and J.L. performed the electrophysiological experiments and analysed the results. R.L. performed the ultrastructural analysis. M.V. and R.P. carried out *in utero* electroporation and *in utero* viral injections, respectively. K.L., R.L., J.L., O.M. and B.R. provided reagents, materials and analysis tools. P.F., O.M. and B.R. discussed the results and wrote the paper.

Author Information Reprints and permissions information is available at www.nature.com/reprints. The authors declare no competing financial interests. Correspondence and requests for materials should be addressed to O.M. (o.marin@umh.es) or B.R. (brico@umh.es).

©2010 Macmillan Publishers Limited. All rights reserved

METHODS

Mice. The generation of mice used in this study has been previously described[31–36]. Mice were maintained at the Instituto de Neurociencias (CSIC-UMH) in accordance with Spanish and EU regulations.

Histology. Mice were anaesthetized with an overdose of sodium pentobarbital and perfused with 4% paraformaldehyde (PFA). Brains were fixed for 2 h at 4 °C, cryoprotected in 30% sucrose in PBS, and cut frozen on a sliding microtome at 40 μm or 160 μm (viral experiments). For immunohistochemistry in embryos, pups were euthanized after cooling and their brains were dissected, fixed overnight in 4% PFA, and cut in the vibratome at 60 μm. All primary and secondary antibodies were diluted in PBS containing 0.25% Triton X-100 and 2% BSA. The following primary antibodies were used: rabbit anti-ErbB4 (1:250, Santa Cruz sc-283), rabbit anti-ErbB4 0618 (1:300, a gift from C. Lai (ref. 37), chicken anti-GFP (1:700, Aves Lab), mouse anti-parvalbumin (1:200, Swant), rat anti-somatostatin (1:200, Millipore), mouse anti-calretinin (1:1,000, Millipore); mouse anti-RFP (1:300, Abcam), mouse anti-GAD65 (1:500, Millipore), rabbit anti-GABA (1:2000, Millipore), rabbit anti-pIκBα (1:1,000; rabbit, Cell Signaling Technology), rabbit anti-calbindin (1:2,000, Swant) and guinea pig anti-VGlut-1 (1:300, Millipore). The secondary antibodies for immunofluorescence were Alexa Fluor-conjugated and purchased from Invitrogen. For indirect immunohistochemistry, sections were incubated with biotinylated secondary antibodies (Vector), diluted 1:200, and processed by the ABC histochemical method (Vector).

Western blot. Mouse cortices were lysated in a buffer containing 50 mM Tris, pH 7.4, 150 mM NaCl, 5 mM EDTA, pH 7.4, 1% Triton X-100, 1 mM VO_4Na_3, 50 mM NaF, 0.5% sodium deoxycholate and Protease Inhibitor Cocktail (Complete, Mini, Roche). Samples were then cleared, denatured and run on 8% SDS–PAGE gels. Gels were electrophoretically transferred onto nitrocellulose membranes (Whatman GmbH). Membranes were blocked with 5% BSA (Sigma) in TBST (20 mM Tris-HCl, pH 7.5, 150 mM NaCl and 0.05% Tween20) for 1 h and probed with primary antibodies (anti-ErbB4 0618, see earlier, 1:1,000) in 5% BSA in TBS, followed by treatment with horseradish-peroxidase-conjugated secondary antibodies and ECL western blotting detection reagents (Immobilon, Millipore). Signals were detected and measured with a luminescent image analyser (LAS-1000PLUS; Fuji-firm).

Virus production and injection. Viral constructs were provided by F. H. Gage and produced ($\sim 10^7$ infecting units per ml) as described before[38]. For infection, recipient pregnant females (E13.5) were anaesthetized with sodium pentobarbital (0.625 mg per 10 g of body weight, intraperitoneally), their uterine horns exposed, and mounted under an ultrasound microscope (VisualSonics) as described elsewhere[39]. A micropipette loaded with a 1:1 mix of *GFP-i-Cre* and mRFP retroviruses was inserted into the MGE under real-time ultrasound imaging guidance and ~100 nl of solution were injected.

Electron microscopy. Electron microscopic examination of immunoreactivity for ErbB4 in the hippocampus of mice was performed as described previously using pre-and postembedding immunogold methods[40]. In brief, brains were perfused with 4% PFA, 0.05% glutaraldehyde, and 15% (v/v) saturated picric acid in 0.1 M phosphate buffer. For pre-embedding immunogold labelling, brain sections (60 μm) were cut on a vibratome and processed for immunohistochemical detection of ErbB4 using silver-enhanced immunogold techniques. For postembedding immunogold labelling, ultrathin sections (70 to 90 nm) from Lowicryl-embedded blocks were cut on an ultramicrotome and processed for immunohistochemical detection of ErbB4. Ultrastructural analyses were performed in a Jeol-1010 electron microscope. For quantification of pre-embedding immunogold preparations, a total surface area of approximately 2,000 μm^2 encompassing the proximal stratum radiatum, the stratum pyramidale and the stratum oriens was analysed in single sections from three different animals. We counted a total of 32 terminals in the AIS, 58 terminals in the soma, and 523 terminals in dendritic spines of pyramidal cells. It should be noted that our quantification probably underestimates the total number of stained synapses, in particular in the AIS and soma, because it was not performed in serial sections (that is, negative axon terminals in a single section might be positive in the next section). For quantification of post-embedding immunogold preparations, a total surface area of approximately 2,400 μm^2 encompassing the proximal stratum radiatum, stratum pyramidale and stratum oriens was analysed in single sections from three different animals. We counted a total of 722 terminals in dendritic spines of pyramidal cells, and 43 asymmetrical synapses (putatively excitatory) on dendritic shafts of interneurons (recognized by the absence of spines and convergence of glutamatergic and GABAergic synapses on the shafts). For estimating background levels in our electron microscopy experiments, we quantified the density of gold particles in places in which ErbB4 staining should be absent, such as mitochondria and the lumen of blood vessels. We observed very low levels of background in both pre-embedding (0.05 ± 0.013 immunogold particles per μm^2) and postembedding (0.045 ± 0.011 immunogold particles per μm^2) immunogold preparations.

Migration controls. To assess the possible migratory defects of interneurons expressing *GFP-i-Cre* in $Erbb4^{F/F}$ embryos, we carried out short-term experiments by infecting embryos at E13.5 and analysing the distribution of infected cells at E15.5. To normalize the variability in the total number of infected cells (which varies from one experiment to another), the migration of infected embryonic interneurons from the MGE to the cortex was measured by expressing the ratio of density of infected cells in the subpallium over the density of infected cells found in the cortex.

To evaluate the existence of migratory defects in *Dlx5/6-Cre-i-GFP*;$Erbb4^{F/F}$ mice, we quantified the number of GFP^+ and $calbindin^+$ interneurons in the pallium of E16.5 embryos. Cell density of GFP^+ and $calbindin^+$ interneurons was measured with Neurolucida software.

Imaging and quantification. ImageJ software was used for image processing and analysis of axonal length and branching, as well as for the quantification of GAD65 buttons on soma and AIS of electroporated neurons. Neurolucida software was used to quantify the density of GAD65 buttons over transfected cells *in vitro*. In brief, we drew the profile of the axons of inhibitory neurons located over the soma of pyramidal cells and counted the number of GAD65-positive boutons along these axons. Bouton density was expressed as the number of boutons per length of these axons. Neurolucida software was also used to draw and analyse the dendritic arbour and the candlesticks of infected chandelier cells. For the candlesticks, we measured length, number of boutons and the 'distance to closest candlestick' parameter. This last measurement indicates the average of the distance between each candlestick and the candlestick that is closest to it. This parameter is considered diagnostic of the overall density of the candlesticks in a given volume.

For the *in vivo* analysis of GAD65 and VGlut-1 immunofluorescence, stainings were performed in parallel with their respective controls. Pictures were taken with an inverted Leica DMIRE2 microscope with a ×63 objective at ×4 digital zoom at 1,024 × 1,024 pixels of resolution. For counting, confocal images were processed with ImageJ software. In brief, we applied background subtraction and enhance contrast. We then run threshold and watershed tools to convert the pictures into 'masks'. The region of interest was defined in the channels GFP, pIκBα (for GAD65) and parvalbumin (for VGlut-1), and the number of particles counted.

To verify the deletion of ErbB4 in *GFP-i-Cre* infected $Erbb4^{F/F}$ interneurons at P30, we stained sections from infected animals for CRE and ErbB4. All 20 GFP^+ interneurons analysed expressed CRE and were negative for ErbB4.

Cell density of $GABA^+$ and $parvalbumin^+$ interneurons was measured with Neurolucida software.

Primary cultures. Hippocampi from E17.5–18.5 mouse embryos were dissected, treated with trypsin and dissociated into single cells by gentle trituration. Cells were resuspended in MEM containing 10% FBS (Invitrogen), 1 mM pyruvate, penicillin–streptomycin and 0.6% glucose, and then plated at a density of 1,000 cells per mm^2 on coverslips coated with 0.5 mg ml^{-1} poly-L-lysine (Sigma). After 2 h, the plating medium was replaced by Neurobasal medium (Invitrogen), penicillin–streptomycin and B27 supplements as described before[41]. Cultures were challenged at 3 DIV with purified NRG1-β1 (PeproTech EC) at 100 nM and fixed at 5 DIV. Pictures were taken with a Leica Microscope DM5000B and analysed with ImageJ software. Neurons were transfected at 7 DIV using Lipofectamine (Invitrogen) according to the manufacturer's instructions. Control neurons were transfected with a plasmid expressing enhanced GFP (pCS2-EGFP; Clontech). The coding sequence *CRD-Nrg1* (ref. 42) was subcloned in an expression vector with a chicken β-actin promoter (pCAGGS) followed by an internal ribosome entry site (IRES) and the GFP coding sequence.

***In utero* electroporation.** Pregnant females were anaesthetized with isofluorane. The uterine horns were exposed and embryos were injected through the uterus wall using pulled capillaries filled with DNA (1.5 μg μl^{-1}) diluted in PBS and coloured with Fast Green (0.5%) (Sigma). Brain ventricles were filled with DNA solution (*pCAGGS-IRES-GFP* or *pCAGGS-CRD-Nrg1-IRES-GFP*) and electroporated (CUY21/CUY650P3/ CUY650P5, Nepa Gene Co.) using a program of 45 V, 50 ms, 950 ms, and five pulses.

Electrophysiology. Transverse hippocampal slices (300 μm) were prepared as described before[43]. The slices were continuously perfused with (in mM) 124 NaCl, 3 KCl, 1.25 KH_2PO_4, 1 $MgSO_4$, 2 $CaCl_2$, 26 $NaHCO_3$, and 10 glucose, pH 7.3 (300 mosM). This solution was supplemented with tetrodotoxin (TTX; 1 μM) and picrotoxin (100 μM) to isolate spontaneous mIPSCs, or APV (50 μM) and LY303070 (25 μM) to isolate mEPSCs. Drugs were applied by gravity, and experiments were performed at room temperature (22–25 °C). Tight-seal (>1 GΩ) whole-cell recordings were obtained from the cell body of stratum oriens interneuron and CA1 pyramidal neurons. Patch electrodes were made from borosilicate glass and had a resistance of 3–5 MΩ when filled with the following (in mM): 130 $CsMeSO_3$, 4 NaCl, 10 HEPES, 0.2 EGTA, 10 TEA, 2 Na_2ATP and 0.5 Na_3GTP, (pH 7.3, 287 mosM). For mIPSCs recordings,

©2010 Macmillan Publishers Limited. All rights reserved

$CsMeSO_3$ was substituted by 130 mM CsCl. Neurons were voltage-clamped at −65 mV using an Axopatch 200A amplifier (Axon Instruments). Series resistance (<20 MΩ) was regularly monitored during recordings, and cells were rejected if resistance changed >15% during the experiment. Data were filtered at 2 kHz, digitalized, and stored on a computer using pClamp 8.0 software. Spontaneous responses (mEPSCs and mIPSCs) were analysed using Mini Analysis Program (Synaptosoft) and statistical differences were evaluated by the two-tailed unpaired Student's *t*-test. For the analysis of the release properties of GABAergic synapses, we recorded IPSCs induced by a train of stimuli (five pulses of 1 mA).

31. Stenman, J., Toresson, H. & Campbell, K. J. Identification of two distinct progenitor populations in the lateral ganglionic eminence: implications for striatal and olfactory bulb neurogenesis. *J. Neurosci.* **23,** 167–174 (2003).
32. Goebbels, S. *et al.* Genetic targeting of principal neurons in neocortex and hippocampus of NEX-Cre mice. *Genesis* **44,** 611–621 (2006).
33. Golub, M. S., Germann, S. L. & Lloyd, K. C. Behavioral characteristics of a nervous system-specific erbB4 knock-out mouse. *Behav. Brain Res.* **153,** 159–170 (2004).
34. López-Bendito, G. *et al.* Preferential origin and layer destination of GAD65-GFP cortical interneurons. *Cereb. Cortex* **14,** 1122–1133 (2004).
35. Gassmann, M. *et al.* Aberrant neural and cardiac development in mice lacking the ErbB4 neuregulin receptor. *Nature* **378,** 390–394 (1995).
36. Tidcombe, H. *et al.* Neural and mammary gland defects in ErbB4 knockout mice genetically rescued from embryonic lethality. *Proc. Natl Acad. Sci. USA* **100,** 8281–8286 (2003).
37. Zhu, X., Lai, C., Thomas, S. & Burden, S. J. Neuregulin receptors, erbB3 and erbB4, are localized at neuromuscular synapses. *EMBO J.* **14,** 5842–5848 (1995).
38. Tashiro, A., Sandler, V. M., Toni, N., Zhao, C. & Gage, F. H. NMDA-receptor-mediated, cell-specific integration of new neurons in adult dentate gyrus. *Nature* **442,** 929–933 (2006).
39. Pla, R., Borrell, V., Flames, N. & Marin, O. Layer acquisition by cortical GABAergic interneurons is independent of Reelin signaling. *J. Neurosci.* **26,** 6924–6934 (2006).
40. Luján, R., Nusser, Z., Roberts, J. D., Shigemoto, R. & Somogyi, P. Perisynaptic location of metabotropic glutamate receptors mGluR1 and mGluR5 on dendrites and dendritic spines in the rat hippocampus. *Eur. J. Neurosci.* **8,** 1488–1500 (1996).
41. Banker, G. A. & Cowan, W. M. Rat hippocampal neurons in dispersed cell culture. *Brain Res.* **126,** 397–425 (1977).
42. Flames, N. *et al.* Short- and long-range attraction of cortical GABAergic interneurons by neuregulin-1. *Neuron* **44,** 251–261 (2004).
43. Christensen, J. K., Paternain, A. V., Selak, S., Ahring, P. K. & Lerma, J. A mosaic of functional kainate receptors in hippocampal interneurons. *J. Neurosci.* **24,** 8986–8993 (2004).

©2010 **Macmillan Publishers Limited. All rights reserved**